

See discussions, stats, and author profiles for this publication at: <https://www.researchgate.net/publication/236635852>

Molecular Dynamics Simulation and Computational Two-Dimensional Infrared Spectroscopic Study of Model Amyloid β -Peptide Oligomers

ARTICLE *in* THE JOURNAL OF PHYSICAL CHEMISTRY A · MAY 2013

Impact Factor: 2.69 · DOI: 10.1021/jp403748z · Source: PubMed

CITATIONS

5

READS

54

3 AUTHORS:



Xu Jun

East China Normal University

2 PUBLICATIONS 12 CITATIONS

[SEE PROFILE](#)



John Z.H. Zhang

East China Normal University, New York Univ...

297 PUBLICATIONS 8,035 CITATIONS

[SEE PROFILE](#)



Yun Xiang

East China Normal University

18 PUBLICATIONS 1,061 CITATIONS

[SEE PROFILE](#)

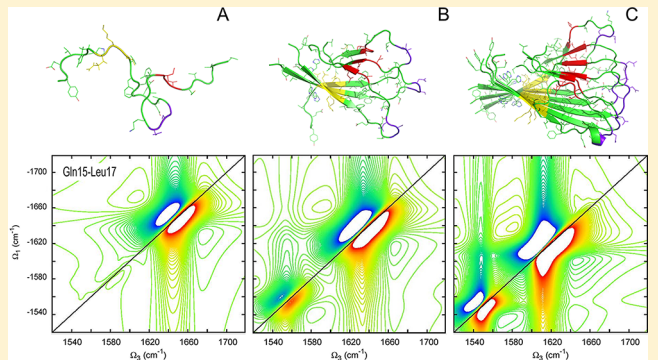
Molecular Dynamics Simulation and Computational Two-Dimensional Infrared Spectroscopic Study of Model Amyloid β -Peptide Oligomers

Jun Xu,[†] John Z. H. Zhang,^{†,‡} and Yun Xiang^{*,†}

[†]State Key Laboratory of Precision Spectroscopy, Department of Physics, Institute of Theoretical and Computational Science, East China Normal University, Shanghai 200062, China

[‡]Department of Chemistry, New York University, New York, New York 10003, United States

ABSTRACT: Molecular dynamics simulations were carried out to study the structure stability of model amyloid β 40 ($A\beta$ 40) peptide oligomers, from monomer to hexamer, in aqueous solution at room temperature. The initial oligomer models were built by using the parallel in-register β -sheet fibril structure and then allowed to relax in the simulations. Our simulation results indicated that the stable $A\beta$ 40 monomer was a random coil, while the oligomer structures became more fibril-like with the increase of the peptide strands. Linear absorption and two-dimensional infrared spectra of the isotope-labeled oligomers were calculated and analyzed in detail, which revealed the differential secondary structural features characteristic of $A\beta$ 40 aggregation. A quantitative relation was established to make connection between the calculated spectra and experimental ensemble measurements.



INTRODUCTION

Protein aggregation in intracellular or extracellular environment could cause serious diseases. Up to now more than 20 human diseases have been found to be associated with protein misfolding and aggregation.^{1–11} Among them, the most common neurodegenerative disease, Alzheimer's disease (AD), is evidently due to the aggregation and deposition of amyloid β peptides ($A\beta$) in patients' brain tissue.^{1,8,11} In this case, the length of the amyloid peptides ranges from 39 to 43 residues, and in healthy humans the particular 40-residue aggregation-prone peptide ($A\beta$ 40) accounts for 90% of the total amyloid peptides. Recent studies have shown that $A\beta$ fibrils form a typical cross- β structure and the β strands stand perpendicular to the fibril axis.^{2,12} However, because of their insoluble and noncrystalline nature, the available techniques such as NMR and X-ray crystallography are not able to directly provide high-resolution structures of amyloid fibrils, hindering our understanding of the structural basis of their pathogenesis mechanism. Moreover, from the perspectives of time resolution, NMR and X-ray techniques only provide average native structures of proteins and do not capture the dynamic pictures of amyloid fibrils' formation. Also, it has become increasingly clear that the most toxic agents that cause neurodegenerative diseases are actually the peptide oligomers and protofibrils.^{3,9,13–18}

One of the popular structure models of $A\beta$ 40 amyloid was proposed by Tycko and co-workers on basis of the structural information obtained from solid-state NMR, atomic force microscopy, and electron microscopy.^{19–23} This model features

a parallel and in-register β -sheet structure including residues 9–24 and 30–40, while residues 25–29 form a loop (see Figure 1). As the detailed atomic structure of $A\beta$ fibrils is not fully resolved and mutational analysis suggested consistent and significant structural malleability,^{24,25} different structural models also have been proposed.²⁶ Extensive experimental and theoretical studies on $A\beta$ protein aggregation have been conducted in recent years.^{27–36}

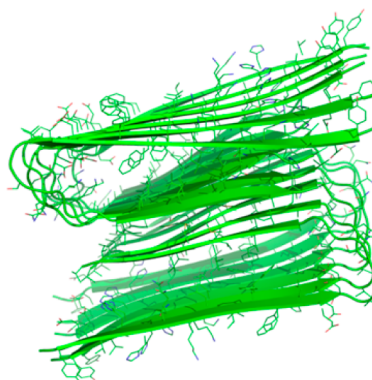


Figure 1. $A\beta$ 40 fibril structure model (PDB code 2LMN).

Special Issue: Prof. John C. Wright Festschrift

Received: April 16, 2013



In the past decade, coherent two-dimensional infrared spectroscopy (2DIR)^{37–51} has emerged as a promising technique that enables us to probe changes in the secondary structure of proteins at unprecedented time resolution, picosecond or even femtosecond. This was made possible by using ultrafast laser pulses. In a protein 2DIR vibrational echo experiment, 3 fs laser pulses are generated to interact with the protein molecules in sequence. The 2DIR spectrum is obtained by a double Fourier transformation of the signal with respect to the time delay between the first pulse and the second pulse, the third pulse and the signal. In the 2DIR spectrum, the amide I (mainly C=O) vibration of the protein backbone and their coupling are shown as diagonal and cross peaks, respectively. Moreover, isotope labeling technique could provide residue-specific information by substituting ¹³C= ¹⁸O for ¹²C= ¹⁶O on certain amide I groups, which lowers the frequency by approximately 60–70 cm⁻¹ and separates the labeled residues from the unlabeled ones.⁵² Recently, extensive 2DIR spectroscopic studies on a number of amyloid fibril systems have been reported from both experiments and theoretical simulations.^{53–58}

Here we reported a computational 2DIR study of the plausible A β 40 oligomer structures in aqueous solution based on the Tycko model (see Figure 1). The starting structures of these oligomers whose number of A β strands ranges from 1 to 6 were constructed by taking the corresponding structures from the Tycko model. Starting from the parallel β -sheet structure, six single-trajectory MD simulations in explicit water solvent at room temperature were performed. The oligomers are allowed to relax and reach equilibrium in 10 ns. As these A β 40 oligomers are built with increasing number of peptide strands, their structural stability and dynamical fluctuation as a function of oligomer size were investigated. Isotope labeling was used to label residues in A β 40's different structure regions, including two β -sheets and a loop, revealing structure information of the labeled regions for the oligomers along aggregation. The 2D infrared spectroscopic signals were calculated using the structures collected in the 10 ns MD simulations. The 2DIR spectra of these A β 40 oligomers with specific labeling regions were compared to gain insight into the aggregation process of the A β fibrils.

THEORETICAL METHODS

a. MD Simulations. The A β_{9-40} peptide fragment studied here has the amino acid sequence GYEVHHQKLVFFAEDV-GSNKGAIIGLMVGGVV. The fibril structure is shown in Figure 1, taken from the Protein Data Bank (PDB) entry 2LMN. The 1–8 residues have been truncated from the structure when constructing the simulation models for this study, as these residues are structurally disordered and have little influence on its aggregation property.^{59,60} (Hereafter for ease of description, we use A β 40 even though A β_{9-40} is actually used in our study.) In order to mimic the aggregation process as closely as possible, we started from an A β 40 monomer and performed an MD simulation at room temperature. Similarly, MD simulations were carried out for the A β 40 dimer, trimer, tetramer, pentamer, and hexamer as well. All the simulations were performed using the NAMD2.8 program⁶¹ with the CHARMM27 force field⁶² for protein and the TIP3P⁶³ water model. The particle mesh Ewald (PME)^{64,65} method was used to treat the long-range electrostatic interactions with the density of grid points of at least 1 Å in all cases. A cutoff of 12 Å was applied to treat the nonbonded van der Waals (VDW) and

electrostatic interactions. Periodic boundary condition (PBC) was imposed on all directions, while the NPT ensemble was adopted. The length of the three dimensions of the simulation water boxes varies from 44.2 to 89.4 Å, depending on the oligomer size. The simulation boxes were extended on each side by 10 Å with water molecules added to fill the space. Langevin dynamics was performed to maintain constant temperature with damping coefficient of 5 ps. The Nose–Hoover Langevin piston^{66,67} method was used to maintain constant pressure with a decay period of 200 fs and an oscillation time of 50 fs. Time step is 2 fs with SHAKE used to constrain all the bonds of hydrogen atoms. The product MD simulations were performed after 2000 energy-minimization steps and last for 10 ns at 300 K.

The root-mean-square deviations (rmsd's) of the protein backbone atoms for the six oligomers are shown in Figure 2. As

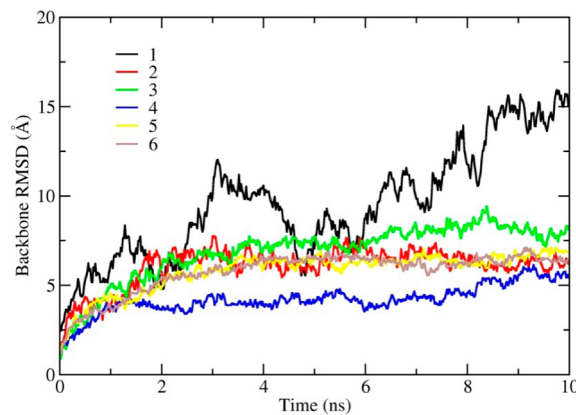


Figure 2. Backbone rmsd as a function of time for the six simulated oligomers (1, monomer; 2, dimer; 3, trimer; 4, tetramer; 5, pentamer; 6, hexamer). The rmsd value was calculated by comparing the running structure with the starting structure.

is clear in the figure, the A β 40 monomer exhibits larger structural fluctuation than all the other simulated oligomers. The oligomers of more peptide strands show much higher stability, and their backbone rmsd values center around 6 Å after equilibrium was reached.

b. Calculation of Linear and 2D IR Spectra. To probe the structure evolution during A β 40 aggregation and to characterize the structural difference between different oligomers via spectroscopic means, the linear absorption and 2DIR spectra were calculated using the software package Spectron^{68,69} for the oligomers. These oligomer structures have reached equilibrium in the simulations, as indicated by the rmsd plateau in Figure 2, except for the monomer, and represent the different intermediates of A β 40 aggregation process. Of course, caution should be taken that these equilibrium states could be only metastable and longer simulations might be needed. Representative structures were selected from the simulated trajectory every 20 ps between 5 and 10 ns, and then the spectra were calculated and averaged over 250 configurations for each oligomer. The linear absorption is given by⁴¹

$$S^1(w) = \sum_e \frac{\Gamma_e |\mu_{eg}|^2}{(\omega - \omega_{eg})^2 + \Gamma_e^2}$$

where ω_{eg} is the frequency of the vibrational excited state e, Γ_e is the homogeneous dephasing rate ($\Gamma_e = 5.5$ cm⁻¹ in our

simulation), and μ_{eg} is the vibrational transition dipole from the ground state to the excited state e . ω_{eg} and μ_{eg} are obtained by using an electrostatic map based on ab initio calculations on the model protein amide unit and parametrization.⁶⁸

The third-order nonlinear response signals were simulated at a parallel laser pulse polarization configuration, and the detected wave vector direction was $K_s = -K_1 + K_2 + K_3$ (vibrational echo) with $t_2 = 0$, where t_2 is the delay time between laser pulses K_2 and K_3 .⁴² In the calculation of the 2D spectra, for each oligomer, the C=O groups of the amide units of the selected residues in three different regions, including two β -sheets and a loop, were labeled with their heavy isotopes ($^{13}\text{C}=\text{O}^{18}$). The fundamental vibrational frequency for each normal amide I mode is set to 1717 cm^{-1} , and its variation due to the electrostatic environment is calculated using the DFT map in ref 68. (eq 9 in ref 68). The fundamental frequency shift of the isotope-substituted amide I vibration is -67 cm^{-1} for $^{13}\text{C}=\text{O}^{18}$ in our simulations. The quasiparticle representation of optical response was used in the 2DIR calculation by solving the nonlinear exciton equations (NEE), which avoided the explicit calculation of the two-exciton states. The third-order nonlinear optical susceptibility $S^3(\omega_3, t_2=0, \omega_1)$ corresponding to vibrational echo was calculated using eq 89 in ref 42 by taking a double Fourier transform of the response function with respect to t_1 and t_3 . The scaling factor for the scattering matrix in NEE is set to 0.3.

RESULTS AND DISCUSSION

The final configurations of the six simulated $\text{A}\beta 40$ oligomers are shown in Figure 3. Obviously, the $\text{A}\beta$ monomer is not able

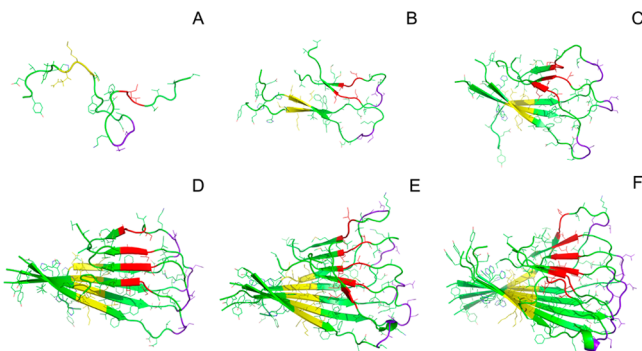


Figure 3. Structure snapshots of the simulated $\text{A}\beta 40$ oligomers. For each oligomer, the structure is taken from the simulated trajectory at $t = 10\text{ ns}$.

to maintain its initial hairpin structure during the simulation. Both large backbone rms fluctuation and the end structure at $t = 10\text{ ns}$ indicate that the monomer has turned into a quite disordered coil. This means that the most stable conformation of $\text{A}\beta 40$ peptide is a random coil instead of the hairpin structure in its fibril form. From the simulation of the dimer, we can see that the two regions in the strands, including residues Gln15-Phe19 and residues Gly33-Met35, started to form two β -sheets in parallel (Figure 3 B), stabilizing the strands in the β -sheet areas while the loop region is still disordered. As the size of the oligomers increases, the β -sheet structure becomes increasingly pronounced. Especially, the β -sheet in the region from Gln15 to Phe19 increased its length drastically as more peptide strands were present in the simulations. Such an elongation of β -sheets reflects the structural reinforcement of

intrastrand connection, and hence, it enhances the stability of these regions.

To make these MD simulation results experimentally comparable, the linear absorption and 2DIR spectra were simulated using a validated protocol^{68,69} based on the structures from the 10 ns simulated trajectories. For each simulated oligomer, the amides of residues in all the $\text{A}\beta$ strands from Gln15 to Leu17 (β -sheet, yellow in Figure 3), Ile32 to Leu34 (β -sheet, red in the figure), Gly25 to Asn27 (loop, purple in the figure) were labeled separately ($^{13}\text{C}=\text{O}^{18}$ substitution for $^{12}\text{C}=\text{O}^{16}$). Since the vibrational frequency for the isotope-labeled amide vibration is red-shifted, we are able to single out those structure regions and make a closer observation. Quantitatively, the $^{13}\text{C}=\text{O}^{18}$ substituted amide I vibration is usually red-shifted by approximately $60\text{--}70\text{ cm}^{-1}$, thus separated from $^{12}\text{C}=\text{O}^{16}$ band of the unlabeled amide groups. The corresponding linear absorption and 2DIR spectra for different oligomers with these three different types of isotope-labeling are calculated. Note that for each spectrum calculation, only one region is labeled, not three simultaneously.

The linear absorption spectra are shown in Figure 4. As we can see from the figure, the absorption band of the amide I ($^{12}\text{C}=\text{O}^{16}$) vibrational modes appears as the major peak, and

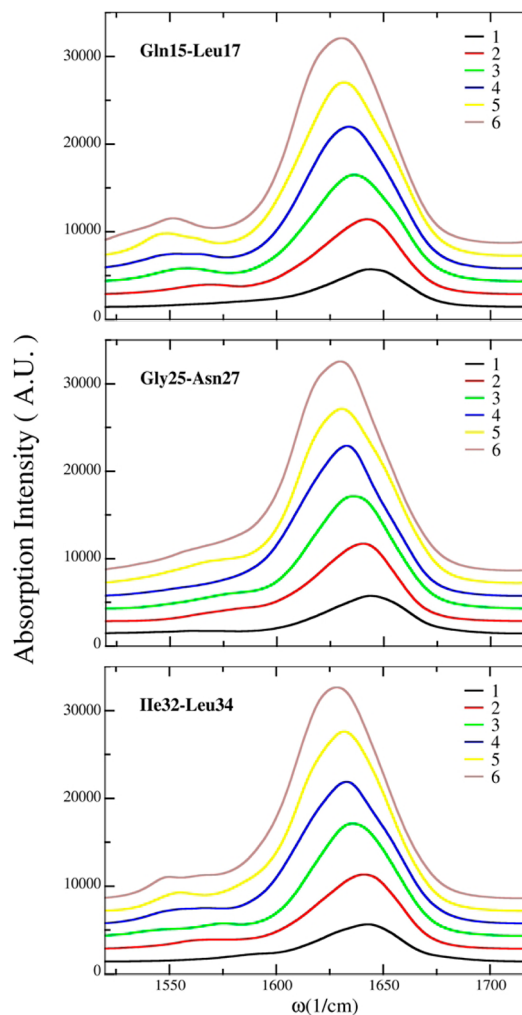


Figure 4. Calculated linear IR spectra for the simulated $\text{A}\beta 40$ oligomers of increasing number of strands with isotope labels at residues in three different regions. AU indicates arbitrary unit.

the minor peak represents the absorption of the isotope-labeled amide I ($^{13}\text{C}=\text{O}$) vibrations. The absorption peak of amide I in the monomer is centered at 1643 cm^{-1} , and the peak position is gradually red-shifted to 1630 cm^{-1} with an increase of the number of strands in the larger oligomers. This can be understood because during the aggregation process, as more and more strands bound together, the formation of the hydrogen bonds between adjacent strands represented by the elongation of β sheets weakens the amide C=O bond appreciably and lowers its vibrational frequency. This is why the peak frequency of the amide I decreases with the growth of $\text{A}\beta40$ fibrils. Moreover, the absorption intensity of $\text{A}\beta40$ oligomers increases as more strands were included in the simulations. The isotope peak intensities in the linear spectra for the two β -sheet region labels are diminishingly weak and even hardly discernible for the loop region labeling for all the oligomers. Moreover, the major amide I peak and the isotope peak are completely congested in the linear spectra.

The calculated 2DIR spectra are shown in Figure 5. Here we present only the imaginary parts of these spectra, as the

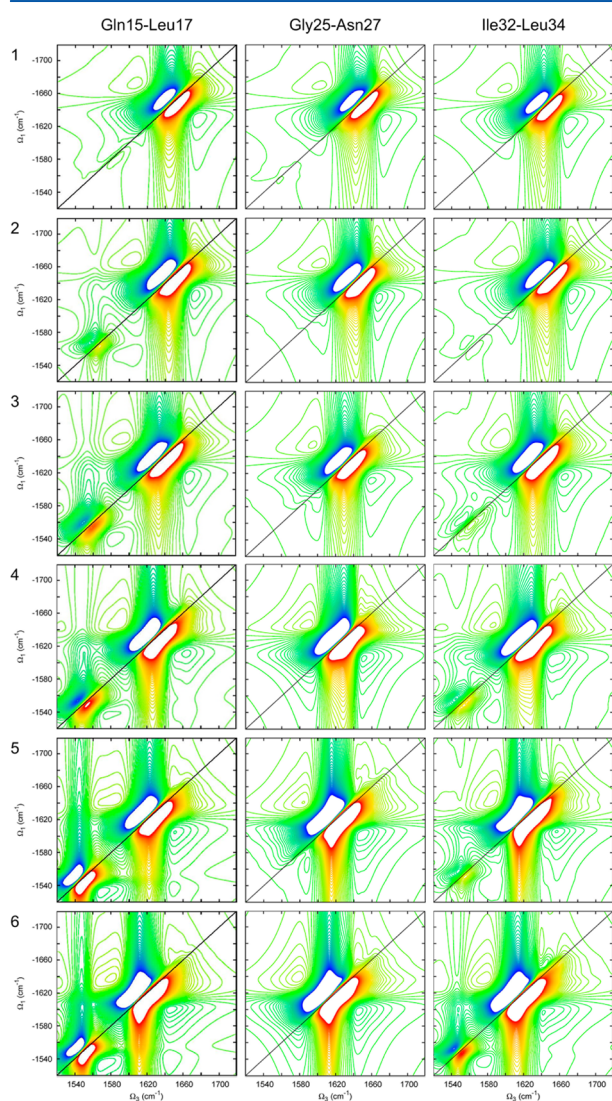


Figure 5. Imaginary parts of the simulated 2DIR vibrational echo spectra for the $\text{A}\beta40$ oligomers labeled at residues in three different regions. The contour level range is chosen to be $[-2, 2]$ to facilitate the comparison of the spectra.

imaginary parts give better comparison for the spectra calculated for different oligomers. The real and absolute magnitude spectra are less representative because of line-shape distortion and broadening but are available upon request. A general trend is observed that the diagonal peaks of the oligomers with more $\text{A}\beta$ strands are significantly broader than those of oligomers of fewer strands. This inhomogeneous broadening arises mostly because more amide I vibrational modes, which are brought by more strands in the simulations, are included in the calculation and those amide groups are in mixed free (such as those in the loop region) and bonded states (such as those in the β -sheets region). Thus, the vibrational frequencies are dispersed.

The main feature in Figure 5 is that in the β -sheet regions the delocalized isotope peak becomes more prominent as more $\text{A}\beta$ peptide strands become available for the oligomers of increasing size and vibration exciton starts to form, while in the loop region the isotope peak does not show up in the simulated spectra. For the monomer, very small isotope diagonal peaks emerge when the amides from Gln15 to Leu17 or the loop region are labeled and there is no isotope peak showing up in labeled residues from Ile32 to Leu34. This reflects the loose and fluctuating coil structure in the monomer. For the dimer, the two β -sheets start to take shape when hydrogen bonds are occasionally forming between the two $\text{A}\beta$ strands while the loop region in the middle still exhibits large fluctuation. From the 2DIR spectra, the isotope peak in the Gln15-Leu17 labeled area becomes stronger in the dimer than in the monomer and this trend applies to the Ile32-Leu34 labeling as well. But the isotope peak intensity is significantly weaker for the Ile32-Leu34 labeling. This is because the coupling between amides in the Gln15-Leu17 labeled region is stronger than that in the Ile32-Leu34 region. Such difference in isotope peak signal intensity between these two labeled regions is also observed in the cases of larger oligomers (i.e., the trimer, tetramer, pentamer, and hexamer). The amide coupling in the loop region between the peptide strands is so weak that no isotope peak is observed. This is mainly due to the structural disorder and lack of hydrogen bonding in the loop region as shown in Figure 3. Overall, the increasing intensity of isotope peaks with the growth of amyloid fibrils suggests the coupling between strands in the labeled β -sheets regions becomes stronger, which is associated with the elongation of β -sheets during aggregation. In addition, the isotope peak of spectra with residues labeled at long β -sheets region (Gln15-Leu17) is more obvious than that of spectra in which short β -sheet region (Ile32-Leu34) is labeled.

The cross peaks originating from the coupling of the labeled amide modes and the $\text{A}\beta40$ main band become visible on the 2DIR spectra of the Gln15-Leu17 labeling and the Ile32-Leu34 labeling for the tetramer, pentamer, and hexamer. For the smaller oligomers, the cross peaks are not recognizable on the calculated spectra. The intensity of the cross peaks is related to the transition dipole distance and orientation of the coupled vibration modes. In our simulations, the coupling scheme is transition dipole coupling for amide I vibrations that are not directly bonded (through space coupling), and an ab initio map is used for the nearest neighbor coupling (through bond coupling). The cross peaks for the main-band–main-band coupled and isotope–isotope coupled amide modes are not observed because of frequency overlap and the high intensity of the diagonal peaks.

The diagonal isotope peak intensity as a function of the number of peptide strands is shown in Figure 6 for the three

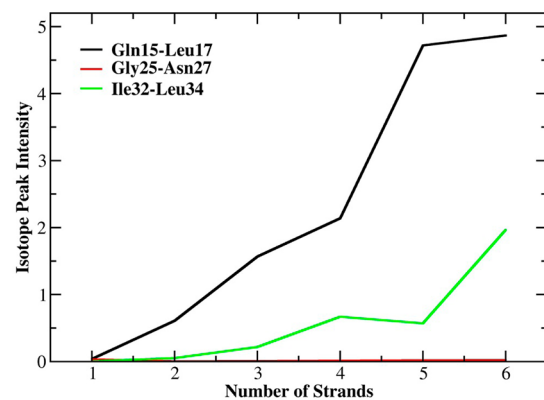


Figure 6. Isotope peak intensity as a function of number of $\text{A}\beta$ strands.

labeling cases, and the corresponding numerical values are tabulated in Table 1. The basic trend is that the isotope peaks intensify as the oligomers grow larger as more peptide strands become available. The N-terminal β -sheet labeling shows a more prominent effect, which indicates the high β -sheet fidelity of this structure region.

Since our spectra are calculated for the pure oligomers in a single-molecule fashion, while in actual experiments all the oligomers could coexist in the same test tube, there is practical difficulty when making a direct comparison between simulation and the ensemble experimental measurement. Because of the nonlinear relation between the isotope peak intensity and oligomer size (i.e., number of peptide strands) shown in Table 1 and Figure 6, the following equation can be established:

$$S_{\text{tot}} = \sum_{n=1}^N S_n = \sum_{n=1}^N k_n C_n$$

which can be used to quantify the relative concentrations of the oligomers in solution. Here, S_{tot} is the experimentally measured total isotope peak intensity, S_n is the intensity of each individual oligomer of size n , k_n are the numbers in a row in Table 1, and C_n is the oligomer number density or concentration. If there are six types of oligomers in the test tube as we simulate in this study ($N = 6$), six different labels and spectroscopic measurements will be needed to set up six linear independent equations. Of course, six sets of spectrum coefficients (i.e., k_n) like those in Table 1 also need to be calculated beforehand. Solving these equations will tell us the relative quantities of the oligomers in solution. Then other thermodynamic parameters such as equilibrium constants can be calculated as well. If the experiments can be carried out time-dependently, then the aggregation rates of the oligomers can also be readily calculated.

CONCLUSIONS

A computational experiment was carried out to investigate the structure stability of the plausible oligomers of $\text{A}\beta40$, one of the peptides responsible for the human neurodegenerative disease AD. The initial structure models of the oligomers were built from the proposed amyloid fibril structure model by Tycko and co-workers. MD simulations were performed to examine the structure evolution of the oligomers in solution (this simulated structure evolution can be viewed as the reverse process of $\text{A}\beta$ oligomerization and aggregation), and their linear absorption and 2DIR spectra with isotope labeling were calculated. The strong isotope spectroscopic signals from the β -sheet regions are consistent with the original structural model based on solid state NMR data. A general trend was observed that as the oligomers grow larger, their structures become more fibril-like and the linear and 2DIR signals intensify accordingly.

A detailed understanding of the microscopic process and molecular mechanism of the aggregation of the amyloid-prone $\text{A}\beta40$ peptide is crucial for developing therapeutic agents for preventing and curing AD. This poses a difficult challenge, since so far experimental studies have not yet been able to capture the oligomers and solve their detailed atomic structures. It remains unclear what are the stable or metastable oligomer species and how they interact with cells and cause cell dysfunction. Our computational effort in this work could shed new light on these issues when the comparison between the simulated 2DIR spectra and experimental results can be made.

AUTHOR INFORMATION

Corresponding Author

*E-mail: xiang@phy.ecnu.edu.cn. Telephone: 86-21-62235467.

Notes

The authors declare no competing financial interest.

ACKNOWLEDGMENTS

This work was supported by the national Natural Science Foundation of China (NSFC, Grants 20903040, 10974054, and 20933002). We thank the supercomputer center at ECNU for computer time.

REFERENCES

- (1) Kang, J.; Lemaire, H. G.; Unterbeck, A.; Salbaum, J. M.; Masters, C. L.; Grzeschik, K. H.; Multhaup, G.; Beyreuther, K.; Muller-Hill, B. The Precursor of Alzheimer's Disease Amyloid A4 Protein Resembles a Cell-Surface Receptor. *Nature* **1987**, 325, 733–736.
- (2) Sunde, M.; Blake, C. C. F. From the Globular to the Fibrous State: Protein Structure and Structural Conversion in Amyloid Formation. *Q. Rev. Biophys.* **1998**, 31, 1–39.
- (3) Caughey, B.; Lansbury, P. T. Protofibrils, Pores, Fibrils, and Neurodegeneration: Separating the Responsible Protein Aggregates from the Innocent Bystanders. *Annu. Rev. Neurosci.* **2003**, 26, 267–298.
- (4) Selkoe, D. J. Folding Proteins in Fatal Ways. *Nature* **2003**, 426, 900–904.

Table 1. Diagonal Isotope Peak Intensities for the Three Labelings in the Simulated 2DIR Spectra for the Six Oligomers

isotope label	diagonal isotope peak intensity (arbitrary unit)					
	monomer	dimer	trimer	tetramer	pentamer	hexamer
Gln15-Leu17	0.038	0.609	1.570	2.142	4.724	4.871
Gly25-Asn27	0.032	0.006	0.007	0.012	0.020	0.021
Ile32-Leu34	0.047	0.050	0.217	0.668	0.569	1.965

- (5) Lester-Coll, N.; Rivera, E. J.; Soscia, S. J.; Doiron, K.; Wands, J. R.; De la Monte, S. M. Intracerebral Streptozotocin Model of Type 3 Diabetes: Relevance to Sporadic Alzheimer's Disease. *J. Alzheimer's Dis.* **2006**, *9*, 13–33.
- (6) Walsh, D. M.; Selkoe, D. J. $\text{A}\beta$ Oligomers—A Decade of Discovery. *J. Neurochem.* **2007**, *101*, 1172–1184.
- (7) Sievers, S. A.; Karanicolas, J.; Chang, H. W.; Zhao, A.; Jiang, L.; Zirafi, O.; Stevens, J. T.; Munch, J.; Baker, D.; Eisenberg, D. Structure-Based Design of Non-Natural Amino-Acid Inhibitors of Amyloid Fibril Formation. *Nature* **2011**, *475*, 96–100.
- (8) Jin, M.; Shepardson, N.; Yang, T.; Chen, G.; Walsh, D.; Selkoe, D. J. Soluble Amyloid Beta-Protein Dimers Isolated from Alzheimer Cortex Directly Induce Tau Hyperphosphorylation and Neuritic Degeneration. *Proc. Natl. Acad. Sci. U.S.A.* **2011**, *108*, 5819–5824.
- (9) Laganowsky, A.; Liu, C.; Sawaya, M. R.; Whitelegge, J. P.; Park, J.; Zhao, M. L.; Pensalfini, A.; Soriaga, A. B.; Landau, M.; Teng, P. K.; et al. Atomic View of a Toxic Amyloid Small Oligomer. *Science* **2012**, *335*, 1228–1231.
- (10) Eisenberg, D.; Jucker, M. The Amyloid State of Proteins in Human Diseases. *Cell* **2012**, *148*, 1188–1203.
- (11) Selkoe, D. J. Preventing Alzheimer's Disease. *Science* **2012**, *337*, 1488–1492.
- (12) Eanes, E. D.; Glenner, G. G. X-ray Diffraction Studies on Amyloid Filaments. *Histochem. Cytochem.* **1968**, *16*, 673–677.
- (13) Kirkitadze, M. D.; Bitan, G.; Teplow, D. B. Paradigm Shifts in Alzheimer's Disease and Other Neurodegenerative Disorders: The Emerging Role of Oligomeric Assemblies. *J. Neurosci. Res.* **2002**, *69*, 567–577.
- (14) Kayed, R.; Head, E.; Thompson, J. L.; McIntire, T. M.; Milton, S. C.; Cotman, C. W.; Glabe, C. G. Common Structure of Soluble Amyloid Oligomers Implies Common Mechanism of Pathogenesis. *Science* **2003**, *300*, 486–489.
- (15) Bitan, G.; Fradinger, E. A.; Spring, S. M.; Teplow, D. B. Neurotoxic Protein Oligomers—What You See Is Not Always What You Get. *Amyloid* **2005**, *12*, 88–95.
- (16) Kodali, R.; Wetzel, R. Polymorphism in the Intermediates and Products of Amyloid Assembly. *Curr. Opin. Struct. Biol.* **2007**, *17*, 48–57.
- (17) Glabe, C. G. Structural Classification of Toxic Amyloid Oligomers. *J. Biol. Chem.* **2008**, *283*, 29639–29643.
- (18) Xue, W. F.; Hellewell, A. L.; Gosai, W. S.; Homans, S. W.; Hewitt, E. W.; Radford, S. E. Fibril Fragmentation Enhances Amyloid Cytotoxicity. *J. Biol. Chem.* **2009**, *284*, 34272–34282.
- (19) Petkova, A. T.; Ishii, Y.; Balbach, J. J.; Antzutkin, O. N.; Leapman, R. D.; Delaglio, F.; Tycko, R. A Structural Model for Alzheimer's Beta-Amyloid Fibrils Based on Experimental Constraints from Solid State NMR. *Proc. Natl. Acad. Sci. U.S.A.* **2002**, *99*, 16742–16747.
- (20) Petkova, A. T.; Yau, W. M.; Tycko, R. Experimental Constraints on Quaternary Structure in Alzheimer's Beta-Amyloid Fibrils. *Biochemistry* **2006**, *45*, 498–512.
- (21) Paravastu, A. K.; Leapman, R. D.; Yau, W. M.; Tycko, R. Molecular Structural Basis for Polymorphism in Alzheimer's Beta-Amyloid Fibrils. *Proc. Natl. Acad. Sci. U.S.A.* **2008**, *105*, 18349–18354.
- (22) Tycko, R.; Leone, S. R.; Cremer, P. S.; Groves, J. T.; Johnson, M. A. Solid-State NMR Studies of Amyloid Fibril Structure. *Annu. Rev. Phys. Chem.* **2011**, *62*, 279–299.
- (23) Luhrs, T.; Ritter, C.; Adrian, M.; Riek-Lohr, D.; Bohrmann, B.; Doeli, H.; Schubert, D.; Riek, R. 3D Structure of Alzheimer's Amyloid-Beta(1–42) Fibrils. *Proc. Natl. Acad. Sci. U.S.A.* **2005**, *102*, 17342–17347.
- (24) Wetzel, R.; Shivaprasad, S.; Williams, A. D. Plasticity of Amyloid Fibrils. *Biochemistry* **2007**, *46*, 1–10.
- (25) Colletier, J. P.; Laganowsky, A.; Landau, M.; Zhao, M. L.; Soriaga, A. B.; Goldschmidt, L.; Flot, D.; Cascio, D.; Sawaya, M. R.; Eisenberg, D. Molecular Basis for Amyloid-Beta Polymorphism. *Proc. Natl. Acad. Sci. U.S.A.* **2011**, *108*, 16938–16943.
- (26) Qiang, W.; Yau, W. M.; Luo, Y. Q.; Mattson, M. P.; Tycko, R. Antiparallel Beta-Sheet Architecture in Iowa-Mutant Beta-Amyloid Fibrils. *Proc. Natl. Acad. Sci. U.S.A.* **2012**, *109*, 4443–4448.
- (27) Fawzi, N. L.; Phillips, A. H.; Ruscio, J. Z.; Doucette, M.; Wemmer, D. E.; Head-Gordon, T. Structure and Dynamics of the $\text{A}\beta_{21–30}$ Peptide from the Interplay of NMR Experiments and Molecular Simulations. *J. Am. Chem. Soc.* **2008**, *130*, 6145–6158.
- (28) Dong, X.; Chen, W.; Mousseau, N.; Derreumaux, P. Energy Landscapes of the Monomer and Dimer of the Alzheimer's Peptide A Beta(1–28). *J. Chem. Phys.* **2008**, *128*, 125108.
- (29) Buchete, N. V.; Hummer, G. Structure and Dynamics of Parallel Beta-Sheets, Hydrophobic Core, and Loops in Alzheimer's A Beta Fibrils. *Biophys. J.* **2007**, *92*, 3032–3039.
- (30) Khandogin, J.; Brooks, C. L. Linking Folding with Aggregation in Alzheimer's Beta-Amyloid Peptides. *Proc. Natl. Acad. Sci. U.S.A.* **2007**, *104*, 16880–16885.
- (31) Dupuis, N. F.; Wu, C.; Shea, J. E.; Bowers, M. T. The Amyloid Formation Mechanism in Human IAPP: Dimers Have Beta-Strand Monomer–Monomer Interfaces. *J. Am. Chem. Soc.* **2011**, *133*, 7240–7243.
- (32) Sgourakis, N. G.; Merced-Serrano, M.; Boutsidis, C.; Drineas, P.; Du, Z. M.; Wang, C. Y.; Garcia, A. E. Atomic-Level Characterization of the Ensemble of the A Beta(1–42) Monomer in Water Using Unbiased Molecular Dynamics Simulations and Spectral Algorithms. *J. Mol. Biol.* **2011**, *405*, 570–583.
- (33) Buell, A. K.; Dhulesia, A.; White, D. A.; Knowles, T. P. J.; Dobson, C. M.; Welland, M. E. Detailed Analysis of the Energy Barriers for Amyloid Fibril Growth. *Angew. Chem., Int. Ed.* **2012**, *51*, 5247–5251.
- (34) Baldwin, A. J.; Knowles, T. P. J.; Tartaglia, G. G.; Fitzpatrick, A. W.; Devlin, G. L.; Shamma, S. L.; Waudby, C. A.; Mossuto, M. F.; Meehan, S.; Gras, S. L.; et al. Metastability of Native Proteins and the Phenomenon of Amyloid Formation. *J. Am. Chem. Soc.* **2011**, *133*, 14160–14163.
- (35) Hayden, E. Y.; Teplow, D. B. Continuous Flow Reactor for the Production of Stable Amyloid Protein Oligomers. *Biochemistry* **2012**, *51*, 6342–6349.
- (36) Tsai, H. H.; Reches, M.; Tsai, C. J.; Gunasekaran, K.; Gazit, E.; Nussinov, R. Energy Landscape of Amyloidogenic Peptide Oligomerization by Parallel-Tempering Molecular Dynamics Simulation: Significant Role of Asn Ladder. *Proc. Natl. Acad. Sci. U.S.A.* **2005**, *102*, 8174–8179.
- (37) Hamm, P.; Lim, M. H.; Hochstrasser, R. M. Structure of the Amide I Band of Peptides Measured by Femtosecond Nonlinear-Infrared Spectroscopy. *J. Phys. Chem. B* **1998**, *102*, 6123–6138.
- (38) Kim, Y. S.; Hochstrasser, R. M. Applications of 2D IR Spectroscopy to Peptides, Proteins, and Hydrogen-Bond Dynamics. *J. Phys. Chem. B* **2009**, *113*, 8231–8251.
- (39) Yan, Y. J.; Mukamel, S. Femtosecond Pump–Probe Spectroscopy of Polyatomic Molecules in Condensed Phases. *Phys. Rev. A* **1990**, *41*, 6485–6504.
- (40) Tanimura, Y.; Mukamel, S. Two-Dimensional Femtosecond Vibrational Spectroscopy of Liquids. *J. Chem. Phys.* **1993**, *99*, 9496–9511.
- (41) Mukamel, S. *Principles of Nonlinear Optical Spectroscopy*; Oxford University Press: New York, 1995.
- (42) Abramavicius, D.; Palmieri, B.; Voronine, D. V.; Sanda, F.; Mukamel, S. Coherent Multidimensional Optical Spectroscopy of Excitons in Molecular Aggregates: Quasiparticle versus Supermolecule Perspectives. *Chem. Rev.* **2009**, *109*, 2350–2408.
- (43) Zheng, J. R.; Kwak, K.; Asbury, J.; Chen, X.; Piletic, I. R.; Fayer, M. D. Ultrafast Dynamics of Solute–Solvent Complexation Observed at Thermal Equilibrium in Real Time. *Science* **2005**, *309*, 1338–1343.
- (44) Fayer, M. D. Fast Protein Dynamics Probed with Infrared Vibrational Echo Experiments. *Annu. Rev. Phys. Chem.* **2001**, *52*, 315–356.
- (45) Jonas, D. M.; Leone, S. R.; Alivisatos, P.; McDermott, A. E. Two-Dimensional Femtosecond Spectroscopy. *Annu. Rev. Phys. Chem.* **2003**, *54*, 425–463.

- (46) Wright, J. C. Coherent Multidimensional Vibrational Spectroscopy. *Int. Rev. Phys. Chem.* **2002**, *21*, 185–255.
- (47) Ganim, Z.; Chung, H. S.; Smith, A. W.; Deflores, L. P.; Jones, K. C.; Tokmakoff, A. Amide I Two-Dimensional Infrared Spectroscopy of Proteins. *Acc. Chem. Res.* **2008**, *41*, 432–441.
- (48) Ge, N. H.; Zanni, M. T.; Hochstrasser, R. M. Effects of Vibrational Frequency Correlations on Two-Dimensional Infrared Spectra. *J. Phys. Chem. A* **2002**, *106*, 962–972.
- (49) Zanni, M. T.; Hochstrasser, R. M. Two-Dimensional Infrared Spectroscopy: A Promising New Method for the Time Resolution of Structures. *Curr. Opin. Struct. Biol.* **2001**, *11*, 516–522.
- (50) Wang, J. P.; Hochstrasser, R. M. Anharmonicity of Amide Modes. *J. Phys. Chem. B* **2006**, *110*, 3798–3807.
- (51) Xiang, Y.; Duan, L. L.; Zhang, J. Z. H. Folding Dynamics of a Small Protein at Room Temperature via Simulated Coherent Two-Dimensional Infrared Spectroscopy. *Phys. Chem. Chem. Phys.* **2010**, *12*, 15681–15688.
- (52) Fang, C.; Wang, J.; Kim, Y. S.; Charnley, A. K.; Barber-Armstrong, W.; Smith, A. B.; Decatur, S. M.; Hochstrasser, R. M. Two-Dimensional Infrared Spectroscopy of Isotopomers of an Alanine Rich Alpha-Helix. *J. Phys. Chem. B* **2004**, *108*, 10415–10427.
- (53) Asplund, M. C.; Zanni, M. T.; Hochstrasser, R. M. Two-Dimensional Infrared Spectroscopy of Peptides by Phase-Controlled Femtosecond Vibrational Photon Echoes. *Proc. Natl. Acad. Sci. U.S.A.* **2000**, *97*, 8219–8224.
- (54) Kim, Y. S.; Liu, L.; Axelsen, P. H.; Hochstrasser, R. M. Two-Dimensional Infrared Spectra of Isotopically Diluted Amyloid Fibrils from A Beta 40. *Proc. Natl. Acad. Sci. U.S.A.* **2008**, *105*, 7720–7725.
- (55) Zhuang, W.; Abramavicius, D.; Voronine, D. V.; Mukamel, S. Simulation of Two-Dimensional Infrared Spectroscopy of Amyloid Fibrils. *Proc. Natl. Acad. Sci. U.S.A.* **2007**, *104*, 14233–14236.
- (56) Shim, S. H.; Strasfeld, D. B.; Ling, Y. L.; Zanni, M. T. Automated 2D IR Spectroscopy Using a Mid-IR Pulse Shaper and Application of This Technology to the Human Islet Amyloid Polypeptide. *Proc. Natl. Acad. Sci. U.S.A.* **2007**, *104*, 14197–14202.
- (57) Falvo, C.; Zhuang, W.; Kim, Y. S.; Axelsen, P. H.; Hochstrasser, R. M.; Mukamel, S. Frequency Distribution of the Amide-I Vibration Sorted by Residues in Amyloid Fibrils Revealed by 2D-IR Measurements and Simulations. *J. Phys. Chem. B* **2012**, *116*, 3322–3330.
- (58) Dunkelberger, E. B.; Buchanan, L. E.; Marek, P.; Cao, P.; Raleigh, D. P.; Zanni, M. T. Deamidation Accelerates Amyloid Formation and Alters Amylin Fiber Structure. *J. Am. Chem. Soc.* **2012**, *134*, 12658–12667.
- (59) Paravastu, A. K.; Petkova, A. T.; Tycko, R. Polymorphic Fibril Formation by Residues 10–40 of the Alzheimer’s Beta-Amyloid Peptide. *Biophys. J.* **2006**, *90*, 4618–4629.
- (60) Buchete, N. V.; Tycko, R.; Hummer, G. Molecular Dynamics Simulations of Alzheimer’s Beta-Amyloid Protofilaments. *J. Mol. Biol.* **2005**, *353*, 804–821.
- (61) Kale, L.; Skeel, R.; Bhandarkar, M.; Brunner, R.; Gursoy, A.; Krawetz, N.; Phillips, J.; Shinozaki, A.; Varadarajan, K.; Schulten, K. NAMD2: Greater Scalability for Parallel Molecular Dynamics. *J. Comput. Phys.* **1999**, *151*, 283–312.
- (62) MacKerell, A. D.; Bashford, D.; Bellott, M.; Dunbrack, R. L.; Evanseck, J. D.; Field, M. J.; Fischer, S.; Gao, J.; Guo, H.; Ha, S.; et al. All-Atom Empirical Potential for Molecular Modeling and Dynamics Studies of Proteins. *J. Phys. Chem. B* **1998**, *102*, 3586–3616.
- (63) Jorgensen, W. L.; Chandrasekhar, J.; Madura, J. D.; Impey, R. W.; Klein, M. L. Comparison of Simple Potential Functions for Simulating Liquid Water. *J. Chem. Phys.* **1983**, *79*, 926–935.
- (64) Essmann, U.; Perera, L.; Berkowitz, M. L.; Darden, T.; Hsing, L.; Pedersen, L. G. A Smooth Particle Mesh Ewald Method. *J. Chem. Phys.* **1995**, *103*, 8577–8593.
- (65) Darden, T.; York, D.; Pedersen, L. Particle Mesh Ewald: an N.log(N) Method for Ewald Sums in Large Systems. *J. Chem. Phys.* **1993**, *98*, 10089–10092.
- (66) Martyna, G. J.; Tobias, D. J.; Klein, M. L. Constant Pressure Molecular Dynamics Algorithms. *J. Chem. Phys.* **1994**, *101*, 4177–4189.
- (67) Feller, S. E.; Yuhong, Z.; Pastor, R. W.; Brooks, B. R. Constant Pressure Molecular Dynamics Simulation: The Langevin Piston Method. *J. Chem. Phys.* **1995**, *103*, 4613–4621.
- (68) Hayashi, T.; Zhuang, W.; Mukamel, S. Electrostatic DFT Map for the Complete Vibrational Amide Band of NMA. *J. Phys. Chem. A* **2005**, *109*, 9747–9759.
- (69) Zhuang, W.; Abramavicius, D.; Hayashi, T.; Mukamel, S. Simulation Protocols for Coherent Femtosecond Vibrational Spectra of Peptides. *J. Phys. Chem. B* **2006**, *110*, 3362–3374.